Geometry-Based Clustering Characteristics for Outdoor Measurements at 28-30 GHz

Zhang, Guojin; Nielsen, Jesper Ødum; Cai, Xuesong; Pedersen, Gert Frølund; Fan, Wei

Published in:
I E E E Antennas and Wireless Propagation Letters

DOI (link to publication from Publisher):
10.1109/LAWP.2022.3180179

Publication date:
2022

Document Version
Accepted author manuscript, peer reviewed version

Geometry-Based Clustering Characteristics for Outdoor Measurements at 28-30 GHz

Guojin Zhang, Jesper Ødum Nielsen, Xuesong Cai, Gert Frølund Pedersen, and Wei Fan

***Abstract*—This paper presents an analysis of channel characteristics for an outdoor scenario at the frequency band of 28-30 GHz. A geometry-based clustering algorithm is proposed to group the measured multipath components (MPCs) from the interaction points on the surrounding walls or objects according to Ray Tracing 3-D simulations, giving results that are more physically interpretable than the traditional clustering algorithms. The cluster-level characteristics at 15 positions along a pre-defined route covering both line-of-sight (LoS) and non-LoS (NLoS) scenarios are investigated. Moreover, power contributions of MPCs with multiple bounces (up to 7 bounces in NLoS scenario) from the interaction objects (IOs) are also investigated.**

***Index terms*—** Millimeter wave, outdoor measurement, geometry-based clustering, dispersion, interaction objects, and radio propagation.

I. Introduction

Millimeter-wave (mm-wave) bands have been widely explored for fifth-generation (5G) communication systems due to the large amount of available frequency spectrum and the possibility to construct large-scale antenna arrays [1]. Despite many research efforts have been made in the areas of mm-wave propagation channel measurements and modeling, long-range outdoor measurements with large-scale arrays are still scarce, due to channel sounding limitations caused by high power attenuation in coaxial cables [2]. As wireless communication performance strongly depends on the propagation environments, accurate channel characterization for outdoor scenario is necessary for the design of future communication systems.

The concept of clusters has been extensively used in channel characterization to group the multipath components (MPCs) with similar delay and angular parameters. However, traditional parameter-based clustering algorithms, such as the KPowerMeans (KPM) algorithm [3] and multipath-component-distance (MCD) threshold algorithm [4], are based on the closeness of propagation parameters, lacking the relation to physical scatterers. In [5], a novel KPM-based clustering algorithm for multiple frequency bands was proposed by utilizing the clustering results at mm-wave bands as an initialization for lower bands with richer MPCs, still without addressing the relation to physical scatterers. To link the clusters to their corresponding physical interaction objects (IOs) in the real environment, a geometry-based clustering algorithm was proposed by the combination of measurement and Ray Tracing (RT) simulation, resulting in a closer match to the measured channels [6]. In [7], [8], a geometry-based clustering and tracking method was proposed according to the scattering points obtained from the measurement-based ray tracer for indoor and outdoor cases. However, only single and double bounces are considered for indoor line-of-sight (LoS) environment in [7], and only single bounce and a 2-D Cartesian coordinate system are considered for a suburban scenario in [8]. For the outdoor scenarios considered in the current work with multiple bounces (up to 7) in non-LoS (NLoS) scenarios, a more sophisticated mapping is needed. In [9], manual clustering for identifying their physical scatterers was combined with an automatic clustering algorithm to detect geometry-based clusters in an outdoor case, leading to a high complexity. In summary, though a few works have been reported, a fully automatic and accurate geometry-based clustering algorithm is still missing in the literature.

To this end, the main contributions and novelties of this paper include: 1) An outdoor measurement campaign conducted with a virtual uniform circular array (UCA) in both LoS and NLoS scenarios is introduced. 2) A fully automatic geometry-based clustering method with a 3-D coordinate map is proposed for complicated outdoor scenarios with multiple bounces, linking the clusters to their corresponding physical IOs. The ability of the UCA used in the measurement to distinguish elevation angles of MPCs is not sufficient. Only delays and azimuths estimated for MPCs can be considered with adequate accuracy. This makes it difficult to obtain the full physical interactions of MPCs with the environment, especially for those with multiple bounces. Therefore, we resort to the assistance of the RT tool to obtain physical interaction properties of each MPCs.[1] 3) Finally, the cluster-level channel characteristics linked to their corresponding physical IOs and power contributions of multiple bounces are investigated.

II. Measurement campaign

The map of the outdoor measurement environment is shown in Fig. 1, including several buildings with bicycle shelter, parking space, and corridor in-between the buildings. A fiber-optic-based vector network analyzer (VNA) channel sounder [2],

G. Zhang, J. Ø. Nielsen, G. F. Pedersen and W. Fan are with the APMS section at the Department of Electronic Systems, Faculty of Engineering and Science, Aalborg University, Aalborg 9220, Denmark (e-mail: guojin@es.aau.dk; jni@es.aau.dk; gfp@es.aau.dk; wfa@es.aau.dk). X. Cai is with the Department of Electrical and Information Technology, Lund University, 22100 Lund, Sweden (email: xuesong.cai@eit.lth.se) (Corresponding author: Xuesong Cai)

[1]It is worth noting that the inaccuracy or missing of elevation information in measurements can make it challenging to distinguish, e.g., MPCs from the LoS direction and the ground reflection. It is always beneficial if the measurement system can well resolve paths in the elevation domain.

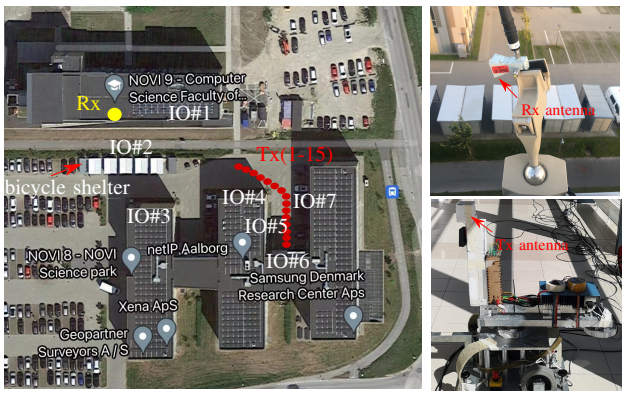

Fig. 1: The measurement environment and channel sounder. (Left) The top-view of the outdoor scenario where the measurement campaign was conducted. Image by Google Maps. (Right-top) Rx antenna on the roof of the building. (Right-bottom) Tx antenna mounted on pedestal used to form the virtual UCA.

[4], [10] was used, allowing long measurement distances up to 300 m and a maximum achievable dynamic range of 112 dB. To increase the signal to noise ratio (SNR), a broadband horn antenna (LB-SJ-180400-KF [11]) was exploited as the receiver antenna (Rx) and fixed on the top of the building at a height of 18 m indicated as the yellow dot in Fig. 1. The main beam of the Rx antenna was down tilted to appropriately cover Tx positions. For the transmitter antenna (Tx) side, an omni-directional biconical antenna [12] was located on a rotating device with a height of 1.15 m above the ground. To form a virtual UCA, the Tx was rotated clockwise in a circle with a radius of 0.25 m and 1° step. For each step, the channel transfer function from 28 GHz to 30 GHz was recorded with 2000 points. The virtual UCA was formed at 15 different positions, as indicated by the red dots in Fig. 1. Position 1-10 are LoS scenarios, and Position 11-15 are NLoS scenarios.

III. Geometry-based clustering method

A. Ray Tracing

The RT tool [13], [14] is used to simulate the radio channels. Besides reflection, diffraction and transmission, diffuse scattering adopting an effective roughness model is also included. The accuracy of the RT tool has been validated in various indoor and outdoor scenarios [13]–[15]. For the simplicity of the simulations, only the outlines of the buildings and the bicycle shelter are modeled. The details of the buildings, such as the windows and the cars in the parking area, are ignored in the simulation. Note that the permittivity and conductivity of the materials in the environment is not completely known, which may lead to inaccurate powers of paths. Nevertheless, the geometry parameters including the delays and angles of the MPCs that are used for clustering in Sect. III-B are well obtained. To lower the computation time, the maximum numbers of reflections and diffraction combined with scattering are set as 4 and 1 for the LoS scenario, while 10 and 5 for the NLoS scenario. The physical interaction properties of each path, such as the IOs (as shown in Fig. 1 with white texts IO#) and the number of bounces, are obtained by the RT tool. When the ground reflections are simulated, it is found that each propagation situation has one more bounce from the ground in the RT simulation with similar delay and azimuth, due to the Tx being close to the ground. Leaving out the extra ground reflection does not affect the accuracy of the initialized clustering centroids described later in Sect. III-B, and is therefore omitted in the simulation for simplicity. Note that the ground reflections exist in the real environment.

B. Cluster centroids initialization

Fig. 2(a) and Fig. 2(d) illustrate the delay-azimuth-power spectra estimated from the measured data at a LoS position 6 and an NLoS position 15, respectively, according to the high-resolution parameter estimation (HRPE) principle in [16], [17]. The minimum MCD principle [4] is used to match the paths identified from the RT simulation to the estimated paths from the measured data exploiting the delays and azimuths of the paths. The MCD threshold $\eta_{\text{MCD},1}$ is used as a threshold distance to limit the search range of matching for a lower complexity. Matched paths identified in the RT simulations at position 6 and position 15 with their corresponding IOs are illustrated in Fig. 2(b) and Fig. 2(e), respectively. It can be observed that all the dominant MPCs estimated from the measured data can be identified in the RT simulation, and only a few weak MPCs are missing. The 3-D propagation mechanisms (plotted in 2-D view for clarity) in the RT simulation for each matched pair are shown in Fig. 2(c) and Fig. 2(f) for the two positions, respectively. The matched paths with the same IO# and the same number of bounces in the RT simulation are grouped as individual clusters. The cluster centroids μ_i are calculated as an initialization for clustering the estimated MPCs in measurements.

C. Main Clustering Algorithm

For each estimated MPC obtained by the HRPE algorithm, the minimum MCD to the RT-initialized cluster centroids is calculated. A MCD threshold $\eta_{\text{MCD},2}$ is exploited to assign estimated MPCs to the RT-initialized clusters or as "new clusters". That is, if the minimum MCD of a path is within $\eta_{\text{MCD},2}$, it is assigned to the nearest RT-initialized cluster centroid. Otherwise, it is labeled as a component of new clusters to be grouped using the MCD threshold-based clustering algorithm [4]. The optimal threshold $\eta_{\text{MCD},2}$ is determined by several cluster validity indices (CVIs). Clusters with powers less than 0.1% of the total power are finally pruned.

Fig. 3(a) and Fig. 3(b) show the clustering results at position 6 and position 15, respectively, with the power in a descending order and the number of bounces indicated in the legend. At position 6, clusters have contributions from LoS, surrounding wall IO#4 and IO#7 as indicated in Fig. 2(c), according to the RT-initialized cluster centroids as shown in Fig. 2(b). However, it is worth noting that Cluster No.3 in Fig. 3(a) is grouped as two clusters if using the traditional MCD threshold clustering method. The clusters at position 15 are contributed by multiple bounces with a maximum order of 7, all occurring in-between the buildings as indicated in Fig. 2(f). It can be observed from Fig. 3(b) that Cluster No.2 and No.4 are

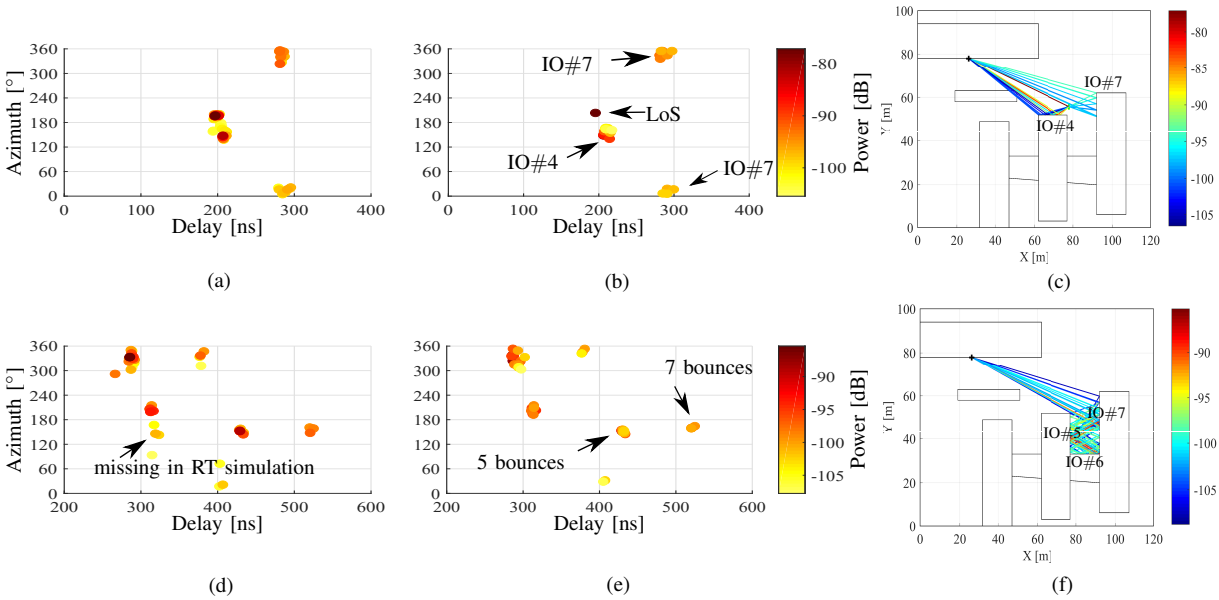

Fig. 2: Example at Position 6 : (a) Delay-azimuth-power spectrum. (b) Matched paths from RT tool. (c) RT map. Example at Position 15 : (d) Delay-azimuth-power spectrum. (e) Matched paths from RT tool. (f) RT map.

close and both have 5 bounces. Nevertheless, they belong to different clusters, as they have different bounce sequence from the surrounding walls as IO#7→IO#5→IO#6→IO#7→IO#5 and IO#7→IO#5→IO#7→IO#6→IO#5, respectively. However, Clusters No.2 and No.4 will be seen as one cluster with the traditional MCD threshold clustering method, as they have similar delays and azimuths. Besides, Cluster No.5 with 7 bounces and Clusters No.2 and No.4 with 5 bounces have higher power than Cluster No.6 with 3 bounces and Cluster No.8 with 4 bounces. Furthermore, the measured MPCs missing in the RT simulation in Fig. 2(d) are grouped as a "new cluster" with unknown bounces and physical IOs, which is Cluster No.7 in Fig. 3(b).

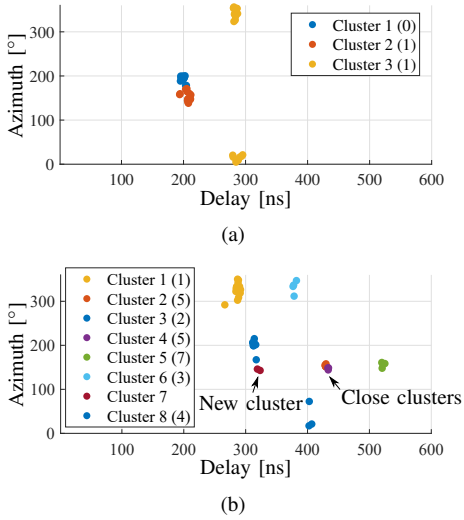

Fig. 3: Clustering results based on the proposed clustering method. (a) Position 6. (b) Position 15.

IV. Cluster-level channel characteristics

A. Multiple bounces

The power percentage of multiple bounces for each Tx position is depicted in Fig. 4(a). New clusters, as defined in Sect. III-C, have unknown numbers of interactions and are marked with -1 for the number of bounces. Since they contribute less than 3% of the total power at each Tx position, they are omitted from the analysis. It can be observed that for the LoS scenario, the power mainly comes from LoS clusters with 0 bounce, while for the NLoS scenario, the power is mostly from single bounce. However, it is seen that the power contribution of LoS cluster at Tx3 is less than that of clusters with one bounce. This is because part of the elements of the large-scale array was blocked in the LoS direction during the measurement. Moreover, it can be observed that the more bounces, the lower the power contribution is, as generally expected. Except in the case of Tx position 15 as shown in Fig. 3(b), the power percentage with 5 bounces is higher than that with 2 and 4 bounces. This possible reason is that the multiple reflections with 5 bounces are mainly from the windows with less power attenuation.

B. Cluster power decay behavior

The cluster power decays versus propagation distances d in logarithmic scale is fitted by the floating-intercept (FI) path loss model [5] with linear regression lines and plotted in Fig. 4(b). The parameters $(\alpha, \beta, \varsigma)$ of the FI path loss model obtained from the MCD-threshold and the proposed methods are also shown in Fig. 4(b). It can be found that the values of the slopes β of the fitting line are similar for the two methods. Additionally, the values of β of both methods are much higher than that found in indoor scenarios at similar frequency bands,

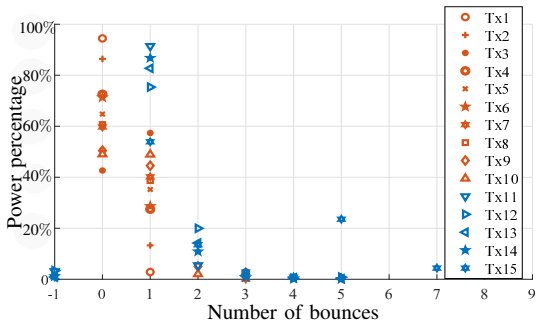

(a)

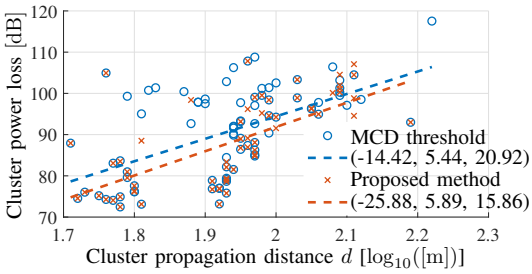

(b)

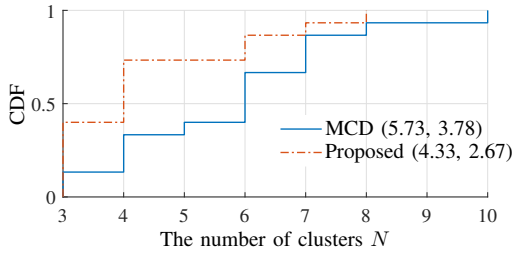

(c)

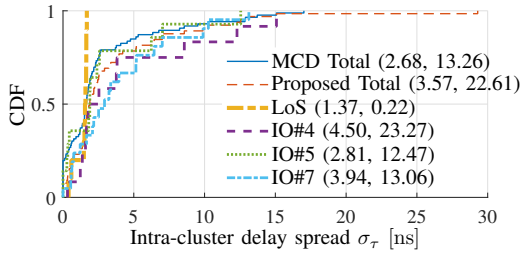

(d)

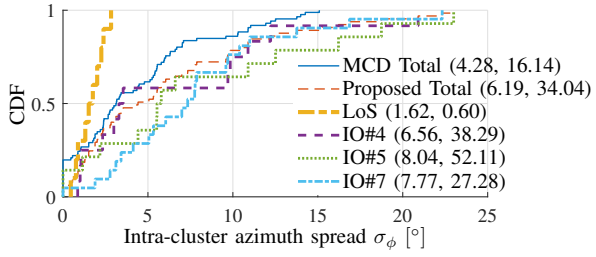

(e)

Fig. 4: Cluster-level parameters. (a) The power percentage of the total power for different number of the bounces. (b) Cluster power loss behaviour. (c) The number of clusters N. (d) Intra-cluster delay spread σ_τ. (e) Intra-cluster azimuth spread σ_ϕ.

which are 2.27 in the classroom, 1.56 in the hall [5], and 3.66 in the NLoS corridor scenario [4]. It means more rapid variations of cluster power versus distance in outdoor scenario. We conjecture that the larger power loss is caused by the multiple bounces occurring between the buildings.

C. The number of clusters

Fig. 4(c) illustrates the CDFs of the number of clusters N [5] of all Tx positions obtained from the MCD-threshold and the proposed methods, with means and variances indicated. The numbers of clusters from both methods are much smaller, compared to those found for LoS indoor scenarios at similar frequency bands, where a mean value of 14.4 was found for the classroom, a mean value of 11 for the hall [5], and a mean value of 21 for the hall and corridor scenario [4] including both LoS and NLoS scenarios. We postulate that it is caused by sparse IOs in outdoor scenarios. Besides, small numbers of clusters, such as less than 4, are mainly in LoS scenario, while a large numbers of clusters usually appear in NLoS scenario, due to the multiple bounces in-between the buildings.

D. Intra-cluster delay and azimuth spread

The CDFs of intra-cluster delay spread σ_τ and azimuth spread σ_ϕ [5] for all the clusters obtained from the MCD-threshold are plotted in Fig. 4(d) and Fig. 4(e). Similarly, the CDFs of σ_τ and σ_ϕ for all the clusters, LoS and the clusters contributed from each IO# obtained from the proposed method are also plotted in Fig. 4(d) and Fig. 4(e). Compared with the results for the indoor scenario in [4], it is found that σ_τ for all the clusters obtained using both clustering methods are much smaller, which are probably caused by the sparse IOs in the outdoor scenario. While it is also found that σ_ϕ for all the clusters are similar, mostly due to the multiple bounces in the corridor in both indoor and outdoor scenarios. It can be observed that both σ_τ and σ_ϕ of LoS clusters are non-zero and smaller than other clusters. This is reasonable, as the Tx is close to the ground, and the reflections from the ground caused non-zero σ_τ and σ_ϕ, while the high power of LoS path compresses the cluster dispersion in both domains. Besides, it can be observed that the clusters from IO#4 have highest σ_τ and lowest σ_ϕ. However, the clusters from IO#5 have lowest σ_τ and highest σ_ϕ. We conjecture this is because the narrow and long dimension in-between IO#5 and IO#7 caused multiple bounces, which enlarges the cluster dispersion in angle domain and leads to smaller delay spread.

V. Conclusions

The geometry-based channel characteristics for the outdoor scenario at the frequency band of 28-30 GHz were investigated in this paper. A geometry-based clustering algorithm was proposed for accurate determination of clusters based on the interaction objects (IOs) obtained from 3D ray tracing (RT) simulations. The complexity and generalization of the proposed algorithm both depend on the RT tool, where only a simplified model was needed. Further research is required for, e.g., THz bands. Using the measured data, cluster-level parameters contributed by different IOs in both line-of-sight (LoS) and non-LoS (NLoS) scenarios were investigated.

REFERENCES

[1] M. Agiwal, A. Roy, and N. Saxena, "Next Generation 5G Wireless Networks: A Comprehensive Survey," *IEEE Communications Surveys Tutorials*, vol. 18, no. 3, pp. 1617–1655, thirdquarter 2016.

[2] A. W. Mbugua, W. Fan, K. Olesen, X. Cai, and G. F. Pedersen, "Phase-Compensated Optical Fiber-Based Ultrawideband Channel Sounder," *IEEE Transactions on Microwave Theory and Techniques*, vol. 68, no. 2, pp. 636–647, 2020.

[3] N. Czink, R. Tian, S. Wyne, F. Tufvesson, J. Nuutinen, J. Ylitalo, E. Bonek, and A. F. Molisch, "Tracking Time-Variant Cluster Parameters in MIMO Channel Measurements," in *the second International Conference on Communications and Networking in China*, Aug 2007, pp. 1147–1151.

[4] X. Cai, G. Zhang, C. Zhang, W. Fan, J. Li, and G. F. Pedersen, "Dynamic Channel Modeling for Indoor Millimeter-Wave Propagation Channels Based on Measurements," *IEEE Transactions on Communications*, vol. 68, no. 9, pp. 5878–5891, 2020.

[5] G. Zhang, J. Nielsen, X. Cai, K. Saito, P. Hanpinitsak, J.-I. Takada, G. F. Pedersen, and W. Fan, "Modeling Multi-Frequency Characteristics for Classroom and Hall Scenarios at 2-4, 9-11 and 27-29 GHz Bands," *IEEE Access*, vol. 9, pp. 14 549–14 563, 2021.

[6] M. Zhu, "Geometry-based Radio Channel Characterization and Modeling: Parameterization, Implementation and Validation," Ph.D. dissertation, Department of Electrical and Information Technology, Lund University, 2014.

[7] P. Hanpinitsak, K. Saito, J.-i. Takada, M. Kim, and L. Materum, "Multipath Clustering and Cluster Tracking for Geometry-Based Stochastic Channel Modeling," *IEEE Transactions on Antennas and Propagation*, vol. 65, no. 11, pp. 6015–6028, 2017.

[8] F. Luan, A. F. Molisch, L. Xiao, F. Tufvesson, and S. Zhou, "Geometrical Cluster-Based Scatterer Detection Method with the Movement of Mobile Terminal," in *2015 IEEE 81st Vehicular Technology Conference (VTC Spring)*, 2015, pp. 1–6.

[9] L. Materum, J.-i. Takada, I. Ida, and Y. Oishi, "Mobile Station Spatio-temporal Multipath Clustering of An Estimated Wideband MIMO Double-directional Channel of A Small Urban 4.5 GHz Macrocell," *EURASIP Journal on wireless communications and networking*, vol. 2009, pp. 1–16, 2009.

[10] W. Fan, A. W. Mbugua, X. Cai, and K. Olesen, "Development and Experimental Validation of an Ultra-wideband Channel Sounder," in *13th European Conference on Antennas and Propagation (EuCAP)*, March 2019, pp. 1–5.

[11] "LB-SJ-180400-KF Datasheet," Tech. Rep. [Online]. Available: http://www.ainfoinc.com.cn/en/pro_pdf/new_products/antenna/Dual%20Polarization%20Horn%20Antenna/tr_LB-SJ-180400.pdf

[12] S. S. Zhekov, A. Tatomirescu, and G. F. Pedersen, "Antenna for Ultrawideband Channel Sounding," *IEEE Antennas and Wireless Propagation Letters*, vol. 16, pp. 692–695, 2017.

[13] V. Degli-Esposti, D. Guiducci, A. de'Marsi, P. Azzi, and F. Fuschini, "An Advanced Field Prediction Model Including Diffuse Scattering," *IEEE Transactions on Antennas and Propagation*, vol. 52, no. 7, pp. 1717–1728, 2004.

[14] V. Degli-Esposti, F. Fuschini, E. M. Vitucci, and G. Falciasecca, "Measurement and modelling of scattering from buildings," *IEEE Transactions on Antennas and Propagation*, vol. 55, no. 1, pp. 143–153, 2007.

[15] A. Karstensen, W. Fan, F. Zhang, J. Ø. Nielsen, and G. F. Pedersen, "Analysis of simulated and measured indoor channels for mm-wave beamforming applications," *International Journal of Antennas and Propagation*, vol. 2018, 2018.

[16] X. Cai and W. Fan, "A Complexity-Efficient High Resolution Propagation Parameter Estimation Algorithm for Ultra-Wideband Large-Scale Uniform Circular Array," *IEEE Transactions on Communications*, vol. 67, no. 8, pp. 5862–5874, Aug 2019.

[17] X. Cai, W. Fan, X. Yin, and G. F. Pedersen, "Trajectory-aided maximum-likelihood algorithm for channel parameter estimation in ultrawideband large-scale arrays," *IEEE Transactions on Antennas and Propagation*, vol. 68, no. 10, pp. 7131–7143, 2020.